J|A|C|S COMMUNICATIONS

Published on Web 06/21/2010

Pt Monolayer on Porous Pd−Cu Alloys as Oxygen Reduction Electrocatalysts†

Minhua Shao,*,‡ Krista Shoemaker,‡ Amra Peles,§ Keiichi Kaneko,# and Lesia Protsailo‡

UTC Power, South Windsor, Connecticut 06074, United Technologies Research Center, East Hartford, Connecticut 06118, and Toyota Motor Engineering & Manufacturing North America Inc., Ann Arbor, Michigan 48105

Received March 8, 2010; E-mail: minhua.shao@utcpower.com

Abstract: We demonstrate the synthesis of a core−shell catalyst consisting of a Pt monolayer as the shell and porous/hollow Pd−Cu alloy nanoparticles as the core. The porous/hollow Pd−Cu nanoparticles were fabricated by selectively dissolving a less noble metal, Cu, using an electrochemical dealloying process. The Pt mass activity for the oxygen reduction reaction of a Pt monolayer deposited on such a porous core is 3.5 times higher than that of a Pt monolayer deposited on bulk Pd nanoparticles and 14 times higher than that of state-of-the-art Pt/C electrocatalysts.

The slow kinetics of the oxygen reduction reaction (ORR) remains a serious challenge for mass production of low-temperature fuel cells that currently require high Pt loading.[1−3] Recent efforts in ORR electrocatalysis have focused on improving the catalytic activity of Pt alloys,[4] minimizing Pt content with a core−shell structure,[5] and replacing Pt by less expensive materials.[6,7] The Pt monolayer catalysts supported on Pd-based cores (Pt/Pd/C) developed in Adzic's group showed higher Pt mass activity than commercial Pt/C catalysts due to the synergistic effect from the core and substantially complete utilization of Pt atoms.[5] The activity of the Pt monolayer strongly depends on the electronic and structural properties of the core.[5a,8] Further enhancing the catalytic activity and stability of the Pt monolayer is of considerable interest,[5a,9] and lowering Pd loading in the core is also of interest. Here we report on porous Pd−Cu alloy nanoparticles formed by an electrochemical dealloying process as the core for the Pt monolayer catalyst, which shows 14 times improvement of the ORR activity of Pt over state-of-the-art Pt/C catalysts. The dealloying method has been used by Strasser's group to synthesize highly active Pt−Cu alloys with a Pt−Cu core and a Pt shell[10] and by Erlebacher's group to fabricate Pt overlayers on nanoporous Au leaf.[11]

Pd−Cu nanoparticles supported on Vulcan XC-72 with a molar ratio of Pd:Cu from 1:2 to 1:12 were prepared by keeping the mixture of 19 wt % Pd/C (BASF) and $Cu(NO_3)_2 \cdot 2.5H_2O$ in an Ar atmosphere at 700 °C for 4 h. A Pd−Cu/C thin film covered with a thin layer of Nafion was casted on a glassy carbon disk (5 mm diameter, Pine Instruments) as the working electrode. Pd−Cu/C was cycled between 0.02 and 1.2 V (vs RHE) for 50 cycles in a N_2-saturated 0.1 M $HClO_4$ solution to achieve a porous structure by leaching out Cu. The Pt monolayer was deposited on the porous core by a Cu-underpotential deposition (UPD)-Pt displacement method.[5a]

A cyclic voltammetry curve (black dashed line) in Figure 1 shows the first cycle of the $PdCu_6$/C during the dealloying process. The high anodic currents at potentials higher than 0.8 V are due to the Cu dissolution from the alloy together with the formation of Pd oxides. A cathodic peak around 0.35 V is ascribed to the re-deposition of Cu. The absence of clear peaks associated with dissolution of bulk Cu suggests that the $PdCu_6$ was well alloyed. The high alloy degree of $PdCu_6$ was confirmed by the X-ray diffraction (XRD) pattern (red line in Figure 2d) that shows a single face-centered cubic phase of Pd−Cu alloy with diffraction angles significantly shifting to higher positions compared to those of Pd/C (black line in Figure 2d). For instance, the (111) peak of Pd−Cu shifts to 42.76° from 40.12° for Pd/C. The particle size and the lattice constant were calculated to be 10.4 and 0.366 nm, respectively, for $PdCu_6$/C and 3.9 and 0.389 nm, respectively, for Pd/C. The alloy degree was very close to 100% based on Vegard's law (Figure S1, Supporting Information (SI)).

After 50 cycles, the hydrogen adsorption/desorption and oxide reduction regions are very similar to those of Pd/C (red line in Figure 1), indicating the formation of a Pd shell. The high-angle annular dark-field transmission electron microscopy (HAADF TEM) images of the $PdCu_6$/C before and after 50 cycles are shown in Figure 2a,b. A large number of nanopores in most of the porous $PdCu_6$ particles were created during the electrochemical cycling. Figure 2c shows several porous $PdCu_6$ particles with pore sizes in the range of 1−5 nm. The inset of Figure 2c is a high-resolution TEM image of a typical porous particle. The formation mechanisms of the nanopores during the electrochemical dealloying require further study. Strasser et al. studied the dealloying process of Pt−Cu alloy nanoparticles, which did not exhibit a porous structure.[12] The XRD pattern of $PdCu_6$/C after dealloying is shown in Figure 2d (blue line). The intensity of the diffraction peak at 42.76° for (111), originating from the $PdCu_6$ alloy, decreases significantly, while a broad peak at 40.59° for (111), corresponding to a lattice constant of 0.385 nm, arises due to the formation of Pd layers or clusters that may still contain very small amounts of Cu since its peak positions are slightly higher than those of pure Pd/C. The remaining $PdCu_6$ alloy diffraction peaks may come from a very small amount of particles with only a small portion of Cu leached (seen as solid particles in Figure 2b). Electron-dispersive spectroscopy (EDS) combined with the HAADF TEM analysis confirmed a much lower Cu content in porous particles than that in solid ones (Figure S2 and Table S1, SI). Inductively coupled plasma mass spectrometry (ICPMS) results showed that ∼85% of Cu atoms in the alloy were leached out during potential cycling.

The voltammetry curve of Pt-monolayer-decorated porous $PdCu_6$/C (Pt/$PdCu_6$/C) is shown in Figure 1 (blue line). Compared with that of $PdCu_6$/C, the oxide formation/reduction peak of Pt/$PdCu_6$/C shifts to a higher potential by 50 mV. This positive potential shift implies a significant oxygen reduction activity enhancement. Figure S3 (SI) displays the ORR polarization curves for Pt/$PdCu_6$/C and Pt/Pd/C in O_2-saturated 0.1 M $HClO_4$ solution, obtained using a rotating disk electrode at 1600 rpm. The curve from Pt/$PdCu_6$/C shows a 40 mV shift to more positive potentials compared with that of Pt/Pd/C. The Pt loading on the electrode for Pt/$PdCu_6$/C was obtained by integrating the Cu UPD charge (Figure S4, SI). The mass ratio of Pt:Pd was found to be ∼1:5, in good agreement with the EDS result (Figure S5, SI). The Pt mass activities of state-of-the-art Pt/C (Tanaka Kikinzoku, 46.4 wt %), Pt/Pd/C, and Pt/$PdCu_6$/C at 0.9 V are 0.2, 0.75, and 2.8 A mg^{-1}, respectively (Figure 3a). Thus, the measured enhancement of Pt mass activity with respect to Pt/C is 14. The specific activities of

† International patent application PCT/US10/00414 related to this work was filed on February 12, 2010.
‡ UTC Power.
§ United Technologies Research Center.
# Toyota Motor Engineering & Manufacturing North America Inc.

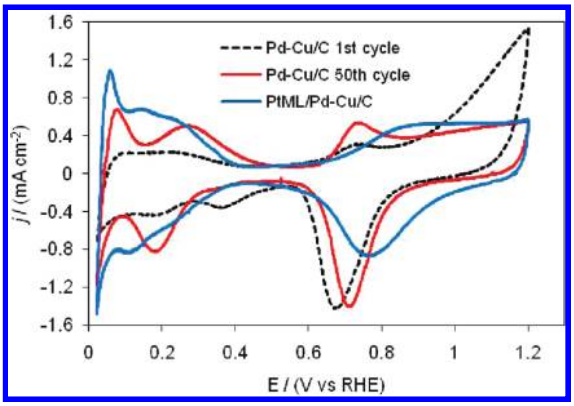

Figure 1. Cyclic voltammograms of $PdCu_6/C$ during the first cycle (black dashed line) and 50th cycle (red line), and a Pt-monolayer-decorated dealloyed $PdCu_6/C$ in N_2-saturated 0.1 M $HClO_4$ solution. Sweep rate, 100 mV s^{-1}; Pd loading, 8 μg cm^{-2}; Pt loading in Pt/$PdCu_6$/C, 1.5 μg cm^{-2}; room temperature.

these catalysts are compared in Figure 3b, which shows that Pt/$PdCu_6$/C is almost 5- and 4-fold more active than Pt/C and Pt/Pd/C, respectively. One may also need to include Pd when comparing the mass activity to account for the cost of this noble metal. The total noble metal activity of Pt/$PdCu_6$/C is 2.3 times higher than that of Pt/C, and the cost equivalent mass activity is 6 times higher, assuming that the cost of Pd is a quarter of that of Pt (Figure S6, SI).

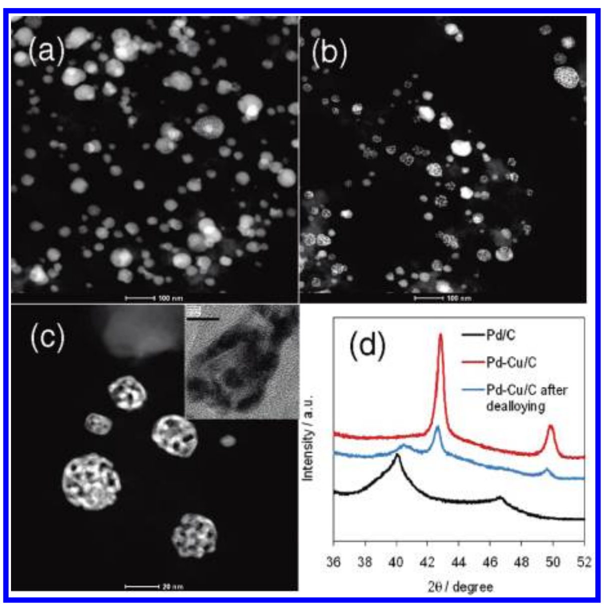

Figure 2. HAADF TEM images of $PdCu_6/C$ before potential cycling (a) and after dealloying (b,c), and XRD patterns of Pd/C and $PdCu_6/C$ before and after dealloying (d). Inset of panel c is a high-resolution TEM image of a typical porous Pd−Cu particle. Scale bars in panels a−c and inset of c are 100, 100, 20, and 10 nm, respectively. For XRD measurements, $PdCu_6/C$ powder was casted on a 1 cm^2 carbon paper with a Pd loading of 0.2 mg cm^{-2}.

Improving the utilization of noble metals in the core is one of the critical steps to further lower the cost of monolayer catalysts. The utilization of Pd atoms in a porous structure is much higher than that of the bulk Pd nanoparticles with a similar size, making the interior atoms of the former available for reactions. For instance, the electrochemically active area of the dealloyed $PdCu_6/C$ is similar to that of the starting material Pd/C, even though the latter has a much smaller particle size. The long-term stability of Pt/$PdCu_6$/C was examined using a square-wave potential cycling protocol at 60 °C in a 0.1 M $HClO_4$ solution, and the results are shown in Figure S7 (SI). The catalysts were cycled, keeping the potential at 0.65 and 1.0 V for 5 s each. After 5000 cycles, the mass activity losses of Pt/$PdCu_6$/C

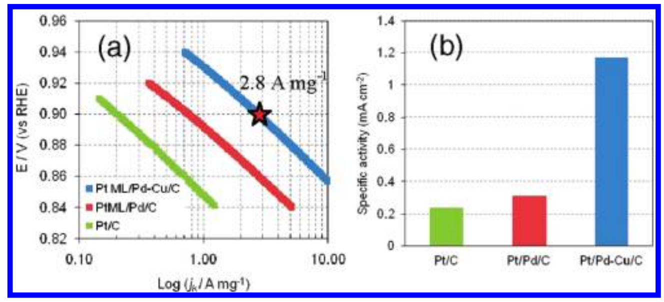

Figure 3. Kinetic currents at 0.9 V normalized to the weight of Pt on the RDE electrode (a) and normalized to the electrochemical active surface areas (b). The surface areas were calculated by integrating the hydrogen adsorption charge in the CVs.

and Pt/C are comparable. No solid particle was found after potential cycling, suggesting the formation of porous structure during cycling.

The XRD and EDS data show that 10−15 atom % of Cu exists in the dealloyed $PdCu_6$ particles. The first one or more layers of the dealloyed $PdCu_6$ particles should consist of pure Pd atoms, and Cu may be found in deeper layers. We infer the presence of a strained Pt layer on the basis of previous findings. Our density functional theory (DFT) calculations (Figure S8, SI) revealed that the oxygen binding energy on a Pt monolayer supported on a $Pd_{0.875}Cu_{0.125}$ alloy core (dealloyed from $PdCu_6$) is 0.15 eV weaker than that on pure Pt due to effects from the compressive strain and electron redistribution between the core and shell. Previous studies concluded that the ORR kinetics on a bulk Pt surface is limited by the rate of removal of strongly adsorbed oxygen-containing species,[8,13,14] which block the adsorption and dissociation sites for oxygen molecules. A slightly lower oxygen binding energy, achieved by lowering the d-band center of Pt, is expected to enhance the ORR activity. Thus, the very high ORR activity of a Pt monolayer on dealloyed Pd−Cu particles can be explained by a lower oxygen binding energy. Similar strain and electronic effects have been observed in the Pt monolayer on a Pd_3Fe core[15] and on Pt (shell)−Pt_xCu (core).[16]

In conclusion, we have demonstrated the synthesis of a porous Pd−Cu alloy core by an electrochemical dealloying process. The ORR activity of a Pt monolayer deposited on such a core is much higher than that of Pt deposited on bulk Pd nanoparticles and 14 times higher than that of state-of-the-art Pt/C electrocatalysts. By increasing the ORR activity and decreasing the noble metal loadings, the cost of fuel cell catalysts could be lowered by 6 times. Further work on these systems will address the optimization of the dealloying process and long-term stability testing in a fuel cell.

Acknowledgment. The authors thank Marianne Pemberton for carrying out some of the experiments.

Supporting Information Available: Experimental procedures and supporting figures. This material is available free of charge via the Internet at http://pubs.acs.org.

References

(1) Gasteiger, H. A.; Kocha, S. S.; Sompalli, B.; Wagner, F. T. *Appl. Catal., B* **2005**, *56*, 9.
(2) Adzic, R. R. In *Electrocatalysis*; Lipkowski, J., Ross, P. N., Eds.; Wiley: New York, 1998; p 197.
(3) Gasteiger, H. A.; Markovic, N. M. *Science* **2009**, *324*, 48.
(4) Stamenkovic, V. R.; Fowler, B.; Mun, B. S.; Wang, G. F.; Ross, P. N.; Lucas, C. A.; Markovic, N. M. *Science* **2007**, *315*, 493.
(5) (a) Adzic, R. R.; Zhang, J.; Sasaki, K.; Vukmirovic, M. B.; Shao, M.; Wang, J. X.; Nilekar, A. U.; Mavrikakis, M.; Valerio, J. A.; Uribe, F. *Top. Catal.* **2007**, *46*, 249. (b) Lim, B.; Jiang, M.; Camargo, P. H. C.; Cho, E. C.; Tao, J.; Lu, X.; Zhu, Y.; Xia, Y. *Science* **2009**, *324*, 130.
(6) Shao, M. H.; Sasaki, K.; Adzic, R. R. *J. Am. Chem. Soc.* **2006**, *128*, 3526.
(7) Lefevre, M.; Proietti, E.; Jaouen, F.; Dodelet, J. P. *Science* **2009**, *324*, 71.
(8) Zhang, J. L.; Vukmirovic, M. B.; Xu, Y.; Mavrikakis, M.; Adzic, R. R. *Angew. Chem., Int. Ed.* **2005**, *44*, 2132.
(9) Zhang, J.; Sasaki, K.; Sutter, E.; Adzic, R. R. *Science* **2007**, *315*, 220.
(10) Koh, S.; Strasser, P. *J. Am. Chem. Soc.* **2007**, *129*, 12624.

(11) Zeis, R.; Mathur, A.; Fritz, G.; Lee, J.; Erlebacher, J. *J. Power Sources* **2007**, *165*, 65.
(12) Strasser, P.; Koh, S.; Greeley, J. *Phys. Chem. Chem. Phys.* **2008**, *10*, 3670.
(13) Xu, Y.; Ruban, A. V.; Mavrikakis, M. *J. Am. Chem. Soc.* **2004**, *126*, 4717.
(14) Stamenkovic, V.; Mun, B. S.; Mayrhofer, K. J. J.; Ross, P. N.; Markovic, N. M.; Rossmeisl, J.; Greeley, J.; Norskov, J. K. *Angew. Chem., Int. Ed.* **2006**, *45*, 2897.
(15) (a) Shao, M. H.; Sasaki, K.; Liu, P.; Adzic, R. R. *Z. Phys. Chem.* **2007**, *221*, 1175. (b) Zhou, W. P.; Yang, X. F.; Vukmirovic, M. B.; Koel, B. E.; Jiao, J.; Peng, G. W.; Mavrikakis, M.; Adzic, R. R. *J. Am. Chem. Soc.* **2009**, *131*, 12755.
(16) Strasser, P.; Koh, S.; Anniyev, T.; Greeley, J.; More, K.; Yu, C.; Liu, Z.; Kaya, S.; Nordlund, D.; Ogaswawra, H.; Toney, M. F.; Nilsson, A. *Nature Chem.* **2010**, *2*, 454.

JA101966A